Chapter 3

Anion fractionation and reactivity at air–water and air–methanol interfaces: implications for the origin of Hofmeister effects*

3.1 Abstract

Anions are selectively enriched in interfacial layers. This universal phenomenon, first identified in connection with protein precipitation 120 years ago, underlies fundamental processes. Its physical causes, however, remain conjectural. It has been speculated that the more polarizable anions should have larger affinities for air/liquid interfaces, and that their reactivities toward gaseous species would be affected by whether the liquid is capped by hydroxyl groups, as in water itself, or by hydrophobic layers of organic contaminants. These issues are particularly relevant to the composition and fate of atmospheric aerosols. Recently we found that fractionation factors f_{X^-} of simple anions at the air/water interface increase exponentially with ion radius a_{X^-}. In this chapter we report new experimental results on a set of anions that include the large PF_6^- and the highly polarizable IO_3^- species. A strict ln $f_{X^-} \propto a_{X^-}$ correlation is confirmed. Experiments performed in $\{x_w\, H_2O + (1 - x_w)\, MeOH\}$ mixtures show that f_{X^-} is almost independent of x_w. Furthermore, $O_3(g)$ oxidizes I^- at virtually identical rates on H_2O and MeOH.

3.2 Introduction

Bromide and particularly iodide are known to be highly enriched in the finest marine aerosol particles.[1-3] This phenomenon has long been ascribed to the binding of halide ions to surface-active organic material,[2] and/or the release of biogenic halocarbon gases from the ocean.[4,5] Since the aerial interfaces of most electrolyte solutions are negatively charged relative to the bulk,[6-8] i.e., anions are selectively enriched at the interface as a matter of course, anion fractionation will inevitably take place during the aerosolization of the ocean upper layers upon bubble breakup.[9,10] Establishing the physical basis of this universal,[11,12] as opposed to contingent or episodic, mechanism of solute fractionation at the air/water interface is key to our understanding of aerosol chemistry[13-15] and its global impact on atmospheric processes.[16,17]

The origin of interfacial ion partitioning is not well understood.[18-20] Electrostatic, hydration, dispersion and hydrophobic forces, hydrogen bonding, and chaotropic/ kosmotropic effects on solvent structure[12,18,20-26] have been invoked to explain specific ion effects. Molecular dynamics and Monte Carlo calculations have revitalized the subject,[15,27,28] using *ab initio* water-water potential energy functions calibrated to account for many-body effects in the bulk.[29] Since the modest enrichment factors (less than an order of magnitude) associated with most interfacial phenomena entail free energy differences $\Delta G \leq 5$ kJ mol^{-1} $\sim 2\,kT$ at 300 K, one may envision multiple explanations for 'anion enrichment'.[19,30,31] A more stringent test for theory and calculations would be to account for robust, quantitative correlations between reliable interfacial fractionation data with ion and/or solvent properties.

The very concept of 'interface', i.e., the depth of what is considered the 'interface' as opposed to the 'interfacial region', is itself ambiguous because it depends on both the phenomenon studied and the probing technique. Surface-specific techniques collect signals from ~ 1 nm deep layers,[32-37] but again, since the free energy gradients associated with interfacial ion enrichment are commensurate with kT, chemically activated processes specifically confined to the 'interface' proper appear to be a contradiction in terms. Perhaps only the fastest reactions, which occur upon heterogeneous reactant encounters could truly probe interfacial structure and dynamics.[38]

In this article, we extend our previous study on anion fractionation[39] to the large PF_6^- and the highly polarizable IO_3^-, and report experimental tests of whether anion fractionation depends on local interfacial properties in water:methanol mixtures, which are largely capped with $-CH_3$ groups above $x_{MeOH} \sim 0.2$.[40-42] We also investigate whether the rates and course of the diffusion-controlled oxidation of interfacial I^- by $O_3(g)$ change from water to methanol.[43-47]

3.3 Experimental Section

NaSCN (98%, Sigma-Aldrich), $NaNO_3$ (99 %, EM Science), NaBr (99.5%, EM Science), $NaBF_4$ (98%, Fluka), $NaClO_4$ (99%, EM Science), NaI (99%, EM Science), $NaPF_6$ (98%, Sigma-Aldrich), and $NaIO_3$ (99%, Sigma-Aldrich) were used as received. Equimolar stock solutions were prepared in purified water (18.2 MΩ cm^{-1} resistivity) from a Millipore Milli-Q Gradient water purification system or in methanol (HRGC grade, EMD Chemicals). Anions at the liquid-air interfaces are directly monitored by electrospray mass spectrometry (ES-MS).[48-50] Equimolar solutions of the sodium salts of various anions were pumped (at 50 μL min^{-1}) into the spraying chamber of the

electrospray mass spectrometer (HP-1100) through a grounded stainless steel needle (100 μm ID, 150 μm OD) surrounded by a coaxial sheath (250 μm ID) that issues N_2(g) at 0.5 L min^{-1}. The large difference between the exit velocities of the liquid jet (10.6 cm s^{-1}) and the N_2 gas (2.65×10^4 cm s^{-1}) forces the liquid to fragment into fine droplets. The spray produced from a grounded nozzle injector consists of a normal distribution of weakly charged microdroplets (centered at zero charge) arising from statistical charge separation during the fragmentation of a neutral liquid. In the electrospray chamber, rapid solvent evaporation leads to the shrinking, and concomitant surface charge crowding of droplets that become mechanically unstable when electric repulsion overtakes liquid cohesion; as a result, they shed their interfacial films to produce finer droplets. This process repeats itself until anions are ultimately field-ejected from the last-generation nanodroplets, and deflected into the mass spectrometer region by applying an appropriate bias to its inlet port. This technique therefore reports the multiplicatively amplified differences in composition of the outermost layers of original droplets. Typical instrumental parameters were: drying gas temperature, 250 ^oC; drying gas flow, 10 L min^{-1}; nebulizer pressure, 35 psi; collector capillary voltage, +3.5 kV; fragmentor voltage, 80 V. Mass spectra were acquired at preset m/z values, 58 and 60 ($^{32,34}SCN^-$), 62 (NO_3^-), 79 and 81 (Br^-), 86 and 87 ($^{10,11}BF_4^-$), 99 and 101 ($^{35,\ 37}ClO_4^-$), 127 (I^-), 145 (PF_6^-), and 175 (IO_3^-). The composition of the interfacial layers of reacting droplets is directly monitored after sub-millisecond contact times, τ, by online electrospray mass spectrometry (ES-MS) of field-ejected anions.[49] Ozone was produced by passing O_2 (g) (ultrapure, Air Liquid America Co.) through an ozone generator (Ozone Solutions), diluted 10-fold with ultrapure N_2 (g), and quantified by a UV-Vis spectrophotometer (Agilent 8452). Ozone concentrations

were calculated from absorbance measurements using recommended values for its absorption cross sections: $\sigma = 1.1 \times 10^{-17}$ (250 nm) and $\sigma = 3.9 \times 10^{-19}$ (300 nm) cm^2 $molecule^{-1}$. The mixed gas was then injected into the chamber, where it was further diluted six-fold by the countercurrent drying gas. Gas flows were regulated by calibrated mass flow controllers (MKS). A schematic diagram of the ozone reaction chamber is shown in Scheme 3.2.

3.4 Results and Discussion

Figure 3.1 shows the negative ion mass spectrum of an electrosprayed equimolar solution of sodium NO_3^-, BF_4^-, ClO_4^-, PF_6^- and IO_3^- salts. Since the technique detects ions already present in solution, Figure 3.1 should display similarly intense signals in the absence of interfacial fractionation. This is clearly not the case. From the mass spectrum of Figure 3.1, normalized anion fractionation factors, f_{X^-}, are calculated from the sum of ion counts, $I_{m/z}$, for the isotopic variants of each anionic species (e.g., $(I_{99} + I_{101})$ for ClO_4^-, etc.) and the total ion count:

$$f_{X^-} = \frac{I_{m/z,X^-}}{\sum I_{m/z,X^-}} \tag{3.1}$$

Thus, by definition, f_{X^-}'s are relative (rather than absolute, i.e., interfacial versus bulk) fractionation factors. They are independent of bulk concentration from 10 to 1000 μM. PF_6^-, which has the largest radius (a_{X^-} = 295 pm) of the set, is exceedingly enriched at the droplet surface. This is consistent with previous surface potential measurements in which PF_6^- displayed a several-fold stronger affinity for the air-water interface than either ClO_4^- or SCN^-.[6] In line with this finding, the smallest anion in the group, IO_3^-, is the least

enriched,[15,34,51,52] despite possessing the largest polarizability (see Table 3-1). The *strict* linearity of the ln f_{X^-} vs. a_{X^-} plots (correlation coefficients $r^2 > 0.98$) of Figure 3.2 demonstrates that the *(negative) free energies associated with the segregation of anions from the bulk solution to the air-liquid interface* (i.e., $f_{X^-} \propto \exp[-{}^{B\rightarrow IF}\Delta G/kT]$) *increase with the first power of ion radius* a_{X^-} [39,53] *rather than with ion volume or polarizability*. Because many ion properties concomitantly depend on ion radius in one way or another, and to avoid confounding cause and effect, we adopted the criterion that the nature of the interactions involved should be sought in the best functional correlation. Thus, since solvation free energies ${}^{S}\Delta G_{X^-} \propto (1/a_{X^-})$ are inversely rather than directly proportional to a_{X^-}[54,55], ln f_{X^-} vs. $-{}^{S}\Delta G_{X^-}$ plots are also quasi-linear (with a negative slope) within a limited range, but they have smaller correlation coefficients than ln f_{X^-} vs. a_{X^-} plots[39]; we therefore reject ${}^{S}\Delta G_{X^-}$ differences as the origin of anion fractionation.

Perhaps unexpectedly, interfacial anion fractionation factors f_{X^-} measured in water/methanol mixtures are weakly dependent on solvent composition over the entire range (Figure 3.3a). Methanol preferentially partitions to the liquid-air interface,[56,57] where water hydroxyls are readily replaced by hydrophobic methyl groups that project into the vapor phase (Figure 3.3b).[41] Thus, we find no experimental grounds to support the hypothesis that interfacial anion fractionation is driven by surface structure or dynamics. By excluding local effects, we realize that any explanation of 'interfacial affinities' becomes conceptually related to Archimedes's principle: lower density bodies float not because they have 'affinity' for the surface, but because the fluid forces them there.[24,25,58-60] We infer that anions are enriched and/or fractionated at air/liquid interfaces

not because they have 'affinity' for these boundaries, but because they are expelled by the whole liquid. The collective underlying interaction in this case is many-body electrodynamic rather than gravitational.

It has been hypothesized that the reactivity of solutes at the air/water interface might be different from in the bulk. This issue arises, for example, in connection with gas-liquid reactions occurring in atmospheric aerosol droplets exposed to reactive gaseous species such as OH-radicals, O_3 or NO_2. Note that, in principle, only the fastest reactions could display 'kinetic surface effects' before the gaseous species have the chance to be solvated and diffuse into the bulk medium. Besides solute fractionation, which expresses preexisting equilibrium interfacial gradients, reactivity is expected to be affected by the state of the solute at the interface, particularly its solvation state, and by the intrinsic asymmetry of an interfacial region open to mass transfer with both the gas-phase and the bulk.

Figure 3.4 shows relative iodide concentrations $[I^-]/[I^-]_0$ at the air-liquid interface as a function of $[O_3(g)]$. We have shown that the initial slopes, S_0, of $[I^-]/[I^-]_0$ vs. $[O_3(g)]$ curves are proportional to the ratio of the second-order-reaction rate constant, k, over the diffusion coefficient D_{I^-} in the condensed phase: $S_0 \propto k/D_{I^-}$.[61] Despite the dissimilar structures of the aerial interfaces of water and methanol, and an estimated ten-fold larger solubility in methanol than in water,[62] $O_3(g)$ oxidizes I^- at identical rates in both solvents: $S_0 = 0.0152 \pm 0.0010$ ppmv^{-1} (H_2O), $S_0 = 0.0145 \pm 0.0002$ ppmv^{-1} (MeOH), regardless of the diverse interactions it may experience upon approaching each surface. Product branching ratios: $\Gamma = [IO_3^-]/[I^-]$, are also similar in water and methanol. By assuming that

$k_3 >> k_2$, $k_5 >> k_4$, the mechanism in Scheme 3.1 implies that Γ should be a linear function of $[O_3(g)]/[I^-]$:[13]

$$\frac{[IO_3^-]}{[I_3^-]} = \frac{k_2}{k_4}\frac{[O_3]}{[I^-]} \tag{3.2}$$

This functional dependence is experimentally confirmed in both solvents, with slopes $(k_2/k_4)_{MeOH} \sim 1.03\ (k_2/k_4)_{water}$ (Figure 3.5a,b). Thus, secondary reactions, which possibly take place in subsurficial layers (such as the one denoted by σ in Figure 3.3b) are also insensitive to the nature of the solvent surface.

Based on the above results and considerations, we propose that the selective enrichment of larger radius anions in air/liquid interfacial layers likely results from rejection by the medium via collective dispersive interactions.[24-26,59,63] The current view is that "the dominant forces on ions in water are short range forces of a chemical nature",[21] i.e., ions hardly perturb the solvent beyond the first solvation shell.[64,65] By strongly binding solvent molecules, the dielectric permittivities of the solvated ions ε_{X^-} are necessarily smaller than that of the bulk solvent's ε_S, except at the air/liquid interface, where $\varepsilon_S(z)$ monotonically falls off to $\varepsilon_S(z) \rightarrow \varepsilon_{air} = 1$ as $z \rightarrow 0$.[66] Electrolyte solutions should be realistically viewed as 'colloidal' suspensions of weakly dielectric, inert solvated ions of radius a_{X^-} in a continuous dielectric medium, rather than intermolecularly perturbed fluids.[65,67,68] Far from the interface, ions remain in a state of indifferent equilibrium, but in the interfacial region, where $\varepsilon_S(z) \rightarrow \varepsilon_{air}$, they experience a net electrodynamic force toward the interface because $\varepsilon_S(z+\delta) > \varepsilon_{X^-} > \varepsilon_S(z-\delta) > 1$.[26,58-60] Furthermore, ions can be treated as large spheres close to the infinite planes separating

solvents from air, and therefore will be repelled toward the interface by many-body dispersion energies that scale with $\sim(a_{X^-}/z)\ [(\varepsilon_{X^-} - \varepsilon_S(z))\ (\varepsilon_{X^-} + \varepsilon_S(z))^{-1}\ (1 - \varepsilon_S(z))\ (1 + \varepsilon_S(z))^{-1}]$ as $z \rightarrow 0$,[25] conforming to the ln f_{X^-} vs. a_{X^-} correlation of Figure 3.2. Notice that if the likely condition $\varepsilon_{X^-} \propto \varepsilon_S$ applies, these energies, which involve dielectric permittivity ratios, are expected to be weakly dependent on absolute ε_S values (cf. Figure 3.3c). How far ions approach, or even protrude into the gas-phase will be ultimately limited, of course, by hydration energy losses. Summing up, interfacial anion fractionation is the electrodynamic equivalent of flotation in a gravitational field, and is determined by ionic radii and solvent permittivity profiles across interfacial layers.

3.5 Acknowledgement

This project was financially supported by the National Science Foundation (ATM-0534990).

3.6 References

(1) Moyers, J. L.; Duce, R. A. *J. Geophys. Res.* **1972**, *77*, 5229.

(2) Duce, R. A.; Hoffman, E. J. *Ann. Rev. Earth Planet. Sci.* **1976**, *4*, 187.

(3) Liss, P. S.; Duce, R. A. *The sea surface and global change*; Cambridge University Press: Cambridge, UK, 1997.

(4) Vogt, R.; Sander, R.; von Glasow, R.; Crutzen, P. J. *J. Atmos. Chem.* **1999**, *32*, 375.

(5) Cicerone, R. J. *Rev. Geophys. Space Phys.* **1981**, *19*, 123.

(6) Randles, J. E. B. *Discuss. Faraday Soc.* **1957**, 194.

(7) Jarvis, N. L. *J. Geophys. Res.* **1972**, *77*, 5177.

(8) Jarvis, N. L.; Scheiman, M. A. *J. Phys. Chem.* **1968**, *72*, 74.

(9) Macintyre, F. *J. Phys. Chem.* **1968**, *72*, 589.

(10) Macintyre, F. *Tellus* **1970**, *22*, 451.

(11) Kunz, W. *Pure Appl. Chem.* **2006**, *78*, 1611.

(12) Kunz, W.; Lo Nostro, P.; Ninham, B. W. *Curr. Opin. Colloid Interface Sci.* **2004**, *9*, 1.

(13) Enami, S.; Vecitis, C. D.; Cheng, J.; Hoffmann, M. R.; Colussi, A. J. *J. Phys. Chem. A* **2007**, *111*, 8749.

(14) Finlayson-Pitts, B. J. *Chem. Rev.* **2003**, *103*, 4801.

(15) Jungwirth, P.; Tobias, D. J. *Chem. Rev.* **2006**, *106*, 1259.

(16) Hunt, S. W.; Roeselova, M.; Wang, W.; Wingen, L. M.; Knipping, E. M.; Tobias, D. J.; Dabdub, D.; Finlayson-Pitts, B. J. *J. Phys. Chem. A* **2004**, *108*, 11559.

(17) Knipping, E. M.; Lakin, M. J.; Foster, K. L.; Jungwirth, P.; Tobias, D. J.; Gerber, R. B.; Dabdub, D.; Finlayson-Pitts, B. J. *Science* **2000**, *288*, 301.

(18) Tobias, D. J.; Hemminger, J. C. *Science* **2008**, *319*, 1197.

(19) Ninham, B. W.; Bostrom, M. *Cell. Mol. Bio.* **2005**, *51*, 803.

(20) Karlstrom, G.; Hagberg, D. *J. Phys. Chem. B* **2002**, *106*, 11585.

(21) Collins, K. D.; Neilson, G. W.; Enderby, J. E. *Biophys. Chem.* **2007**, *128*, 95.

(22) Ninham, B. W.; Yaminsky, V. *Langmuir* **1997**, *13*, 2097.

(23) Gavryushov, S.; Linse, P. *J. Phys. Chem. B* **2003**, *107*, 7135.

(24) van Oss, C. J.; Absolom, D. R.; Neumann, A. W. *Coll. Surf.* **1980**, *1*, 45.

(25) Parsegian, V. A. *Van der Waals Forces*; Cambridge University Press: New York, 2006.

(26) Dzyaloshinskii, I.E.; Lifshitz, E. M.; Pitaevskii, L. P. *Adv. Phys.* **1961**, *10*, 165.

(27) Frediani, L.; Mennucci, B.; Cammi, R. *J. Phys. Chem. B* **2004**, *108*, 13796.

(28) Garrett, B. C. *Science* **2004**, *303*, 1146.

(29) Stone, A. J. *Science* **2007**, *315*, 1228.

(30) Pegram, L. M.; Record, M. T., Jr. *Proc. Natl. Acad. Sci. USA* **2006**, *103*, 14278.

(31) Pegram, L. M.; Record, M. T., Jr. *J. Phys. Chem. B* **2007**, *111*, 5411.

(32) Petersen, P. B.; Johnson, J. C.; Knutsen, K. P.; Saykally, R. J. *Chem. Phys. Lett.* **2004**, *397*, 46.

(33) Petersen, P. B.; Saykally, R. J. *Chem. Phys. Lett.* **2004**, *397*, 51.

(34) Petersen, P. B.; Saykally, R. J. *Annu. Rev. Phys. Chem.* **2006**, *57*, 333.

(35) Petersen, P. B.; Saykally, R. J. *J. Am. Chem Soc.* **2006**, *127*, 15446.

(36) Smith, J. D.; Saykally, R. J.; Geissler, P. L. *J. Am. Chem. Soc.* **2007**, *129*, 13847.

(37) Wilson, K. R.; Rude, B. S.; Smith, J.; Cappa, C.; Co, D. T.; Schaller, R. D.; Larsson, M.; Catalano, T.; Saykally, R. J. *Rev. Sci. Instrum.* **2004**, *75*, 725.

(38) Davidovits, P.; Kolb, C. E.; Williams, L. R.; Jayne, J. T.; Worsnop, D. R. *Chem. Rev.* **2006**, *106*, 1323.

(39) Cheng, J.; Vecitis, C. D.; Hoffmann, M. R.; Colussi, A. J. *J. Phys. Chem. B* **2006**, *110*, 25598.

(40) Prtay, L. B.; Jedlovszky, P. I.; Vincze, A.; Horvai, G. *J. Phys. Chem. B* **2008**.

(41) Chen, H.; Gan, W.; Lu, R.; Guo, Y.; Wang, H. F. *J. Phys. Chem. B* **2005**, *109*, 8064.

(42) Liu, W. T.; Zhang, L. N.; Shen, Y. R. *J. Chem. Phys.* **2006**, *125*, 6.

(43) Liu, Q.; Schurter, L. M.; Muller, C. E.; Aloisio, S.; Francisco, J. S.; Margerum, D. W. *Inorg. Chem.* **2001**, *40*, 4436.

(44) Donaldson, D. J.; Vaida, V. *Chem. Rev.* **2006**, *106*, 1445.

(45) Krisch, M. J.; D'Auria, R.; Brown, M. A.; Tobias, D. J.; Hemminger, J. C.; Ammann, M.; Starr, D. E.; Bluhm, H. *J. Phys. Chem. C* **2007**, *111*, 13497.

(46) Smoydzin, L.; von Glasow, R. *Atmo. Chem. Phys.* **2007**, *7*, 5555.

(47) Cwiklik, L.; Andersson, G.; Dang, L. X.; Jungwirth, P. *Chemphyschem* **2007**, *8*, 1457.

(48) Kebarle, P. *J. Mass Spectrom.* **2000**, *35*, 804.

(49) Kebarle, P.; Peschke, M. *Anal. Chim. Acta* **2000**, *406*, 11.

(50) Kebarle, P.; Tang, L. *Anal. Chem.* **1993**, *65*, A972.

(51) Mucha, M.; Frigato, T.; Levering, L. M.; Allen, H. C.; Tobias, D. J.; Dang, L. X.; Jungwirth, P. *J. Phys. Chem. B* **2005**, *109*, 7617.

(52) Tuma, L.; Jenicek, D.; Jungwirth, P. *Chem. Phys. Lett.* **2005**, *411*, 70.

(53) Eggimann, B. L.; Siepmann, J. I. *J. Phys. Chem. C* **2008**, *112*, 210.

(54) Ashbaugh, H. S. *J. Phys. Chem. B* **2000**, *104*, 7235.

(55) Marcus, Y. *Ion Properties*; Marcel Dekker: New York, 1997.

(56) Chang, T. M.; Dang, L. X. *J. Phys. Chem. B* **2005**, *109*, 5759.

(57) Wolfrum, K.; Graener, H.; Laubereau, A. *Chem. Phys. Lett.* **1993**, *213*, 41.

(58) Israelachvili, J. N. *Quart. Rev. Biophys.* **1974**, *6*, 341.

(59) Israelachvilii, J. *Intermolecular & Surface Forces*, 2nd ed.; Academic Press: London, 1992.

(60) Israelachvilii, J.; Wennerstrom, H. *Nature* **1996**, *379*, 219.

(61) Enami, S.; Hoffmann, M. R.; Colussi, A. J. *Proc. Natl. Acad. Sci. U.S.A.,* **2008**, *105,* 7365.

(62) Bin, A. K. *Ozone-Science & Engineering* **2006**, *28*, 67.

(63) van Oss, C. J.; Chaudhury, M. K. *Chem. Rev.* **1988**, *88*, 927.

(64) Omta, A. W.; Kropman, M. F.; Woutersen, S.; Bakker, H. J. *Science* **2003**, *301*, 347.

(65) Bakker, H. J. *Chem. Rev.* **2008**, *108*, 1456.

(66) Hildebrandt, A.; Blossey, R.; Rjasanow, S.; Kohlbacher, O.; Lenhof, H. P. *Phys. Rev. Lett.* **2004**, *93*, 108104.

(67) Bakker, H. J.; Kropman, M. F.; Omta, A. W. *J. Phys. Condens. Matter* **2005**, *17*, S3215.

(68) Grossfield, A. *J. Chem. Phys* **2005**, *122*, 024506.

(69) Akerlof, G. *J. Am. Chem. Soc.* **1932**, *54*, 4125.

(70) Baumgartner, E.; Busch, M.; Fernandez, R. *J. Phys. Chem.* ***1970,*** 74*, 1821.*

Table 3.1. Interfacial affinities and molecular properties of anions [55]

Anion X^-	Affinities f_{X^-} [a]	Radii a_{X^-} (10^{-12} m)	Dehydration Energies (kJ mol^{-1})	Polarizability (10^{-30} m^3)	Ion Volume (cm^3 mol^{-1})
IO_3^-	0.0103	181	408	7.41	30.8
NO_3^-	0.0149	206 [b]	306	4.20	34.5
BF_4^-	0.0661	230	200	2.78	50.6
ClO_4^-	0.0814	240	214	4.99	49.6
PF_6^-	0.8273	295 [70]	-	4.36 [c]	58.0

a. See text for definition
b. Equatorial radius
c. Value for SiF_6^{2-}

Figure 3.1. ES-MS of a 10 μM equimolar aqueous solution of the sodium salts of the following anions: NO_3^-, BF_4^-, ClO_4^-, PF_6^-, and IO_3^- at pH = 6.5. Ion signal intensities are normalized to total ion intensity.

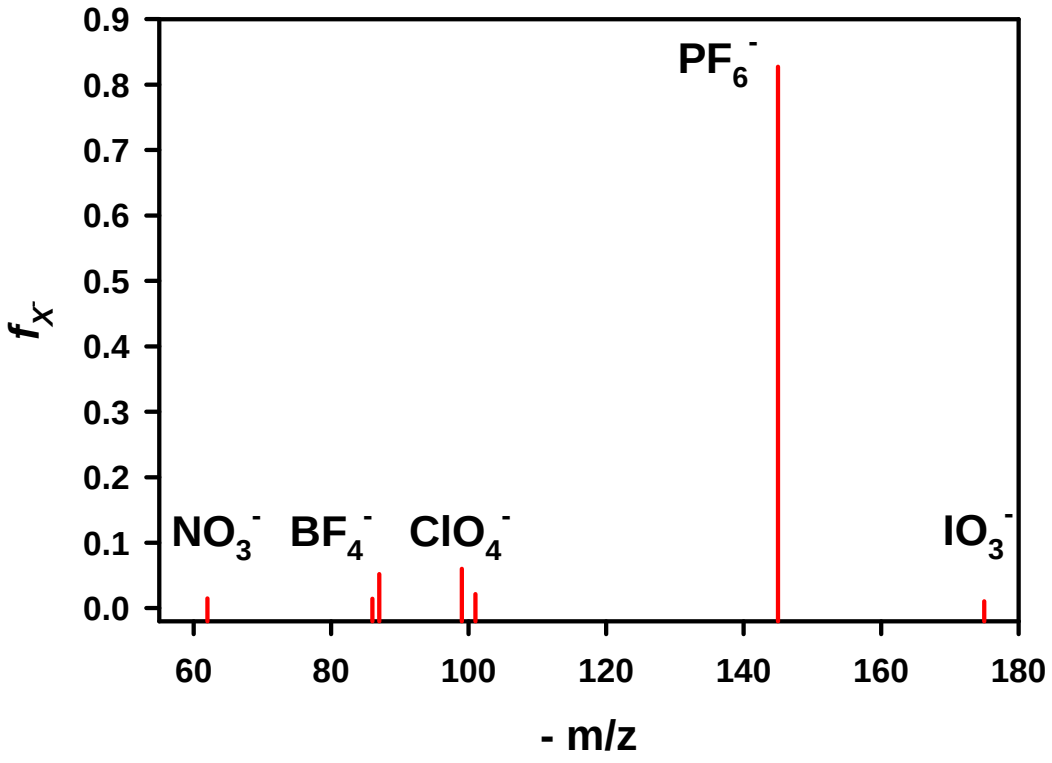

Figure 3.2. Symbols: Normalized anion affinities, f_{X^-} versus crystalline ion radii,a_{X^-}. Solid line: linear regression of ln f_{X^-} vs. a_{X^-}.

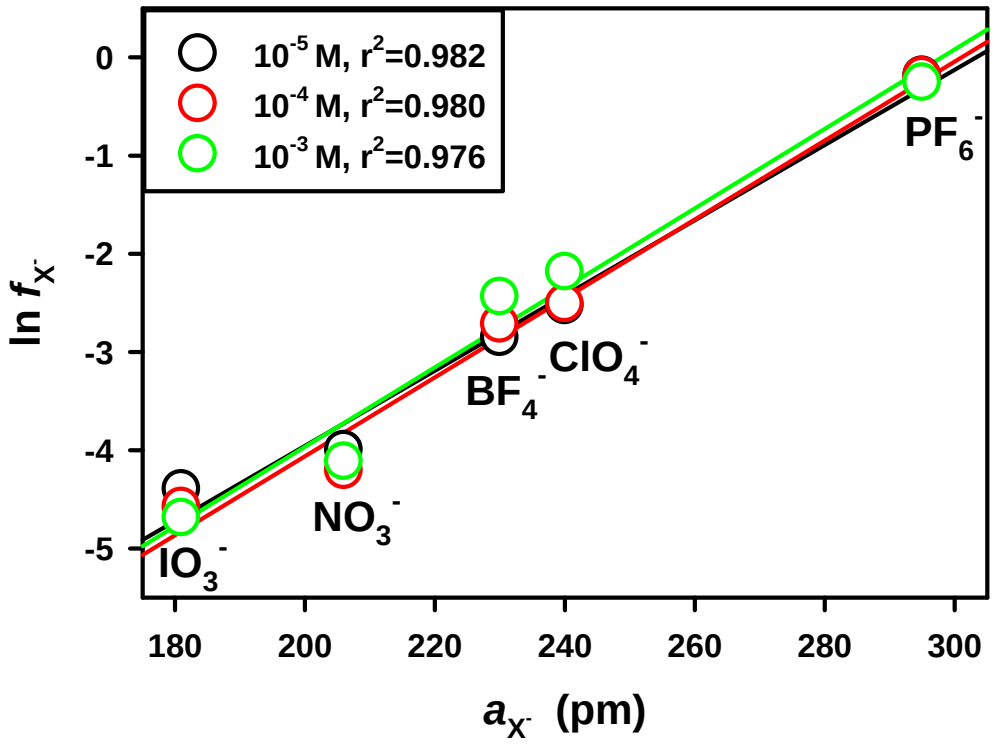

Figure 3.3. (a) f_{X^-} measured in 10 μM solutions of the sodium salts of the corresponding anions; (b) the fractional coverage of -CH_3 groups at the surface, ϑ, and in the layer beneath, σ;[41] (c) the dielectric permitivity of the solvent,[69] as functions of methanol molar fraction in water:methanol mixtures.

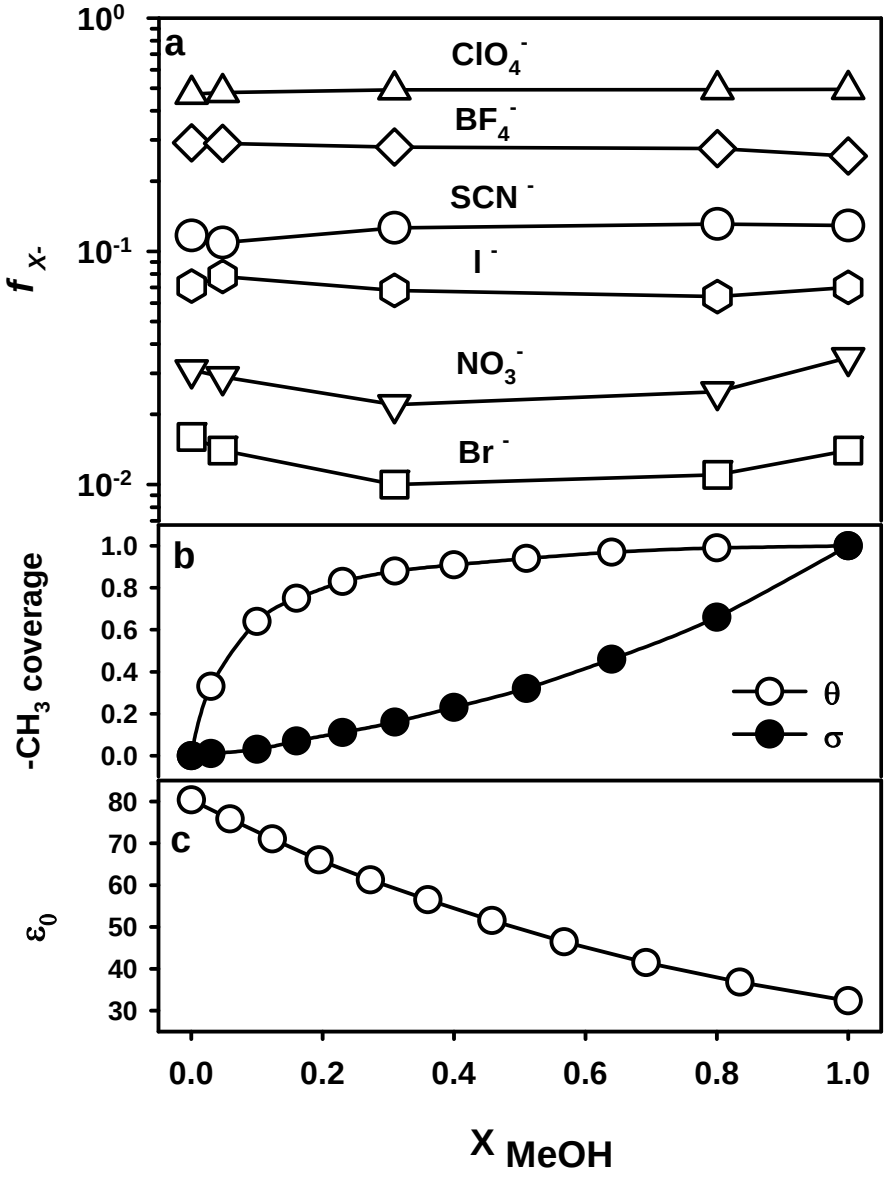

Figure 3.4. Symbols: normalized interfacial iodide concentration $[I^-]/[I^-]_0$ versus $[O_3(g)]$ in (a) H_2O and (b) MeOH; $[I^-]_0$= 10 μM. The data are fitted with exponential decay curves ($r^2 > 0.99$).

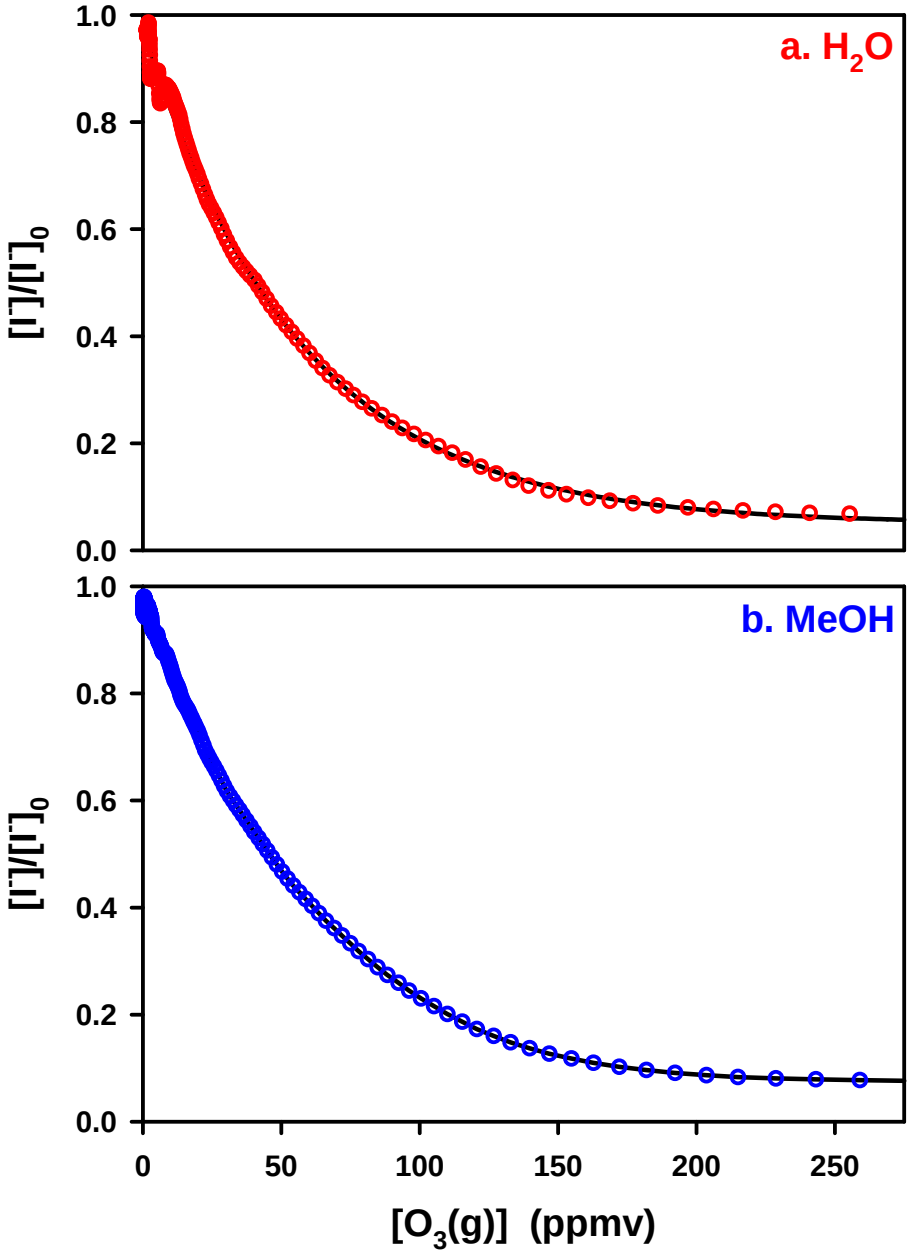

Figure 3.5. The product branching ratio $[IO_3^-]/[I_3^-]$ as a function of $[O_3(g)]/[I^-]$ in (a) H_2O and (b) MeOH; $[I^-]_0$ = 100 μM.

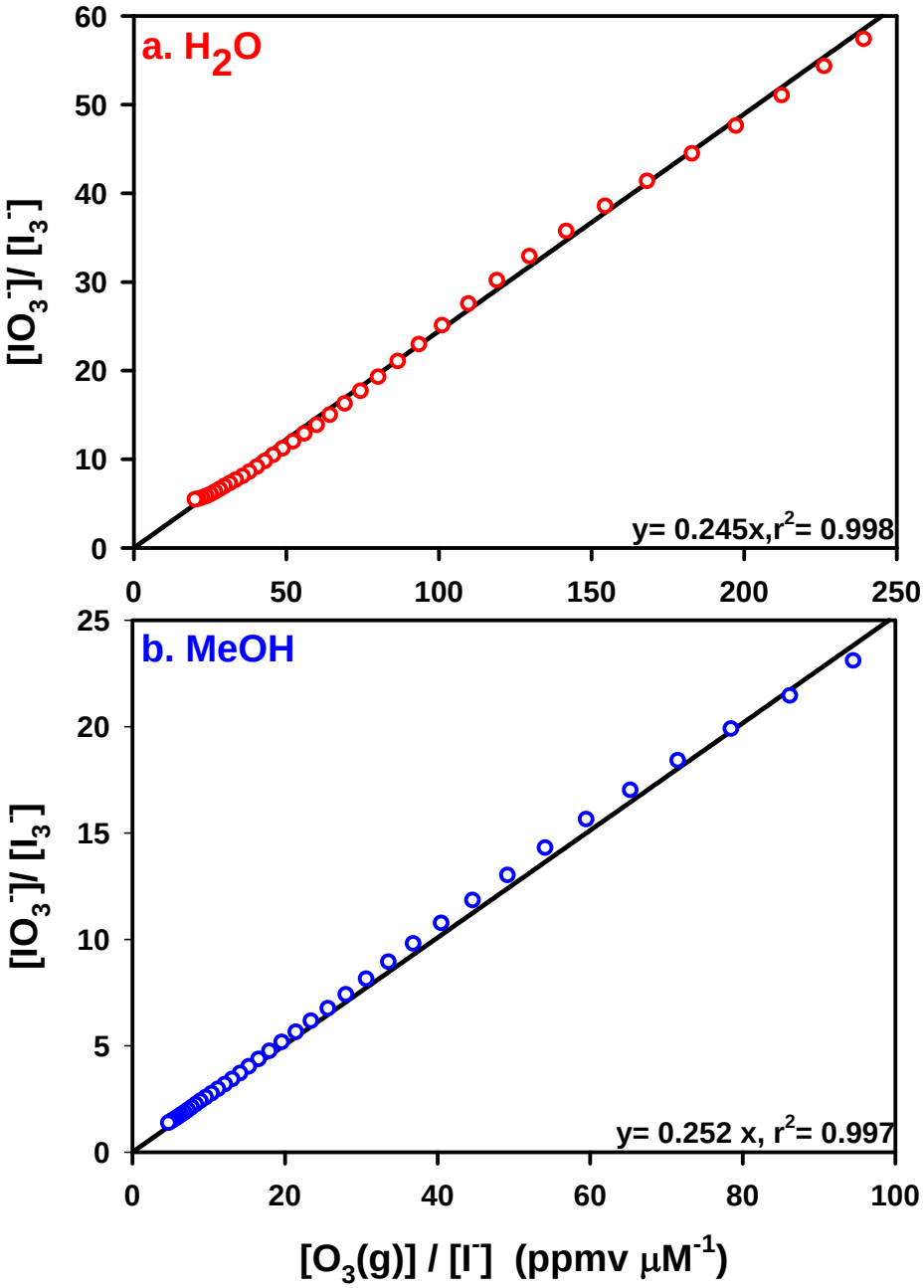

Scheme 3.1. Iodide oxidation by ozone in water.

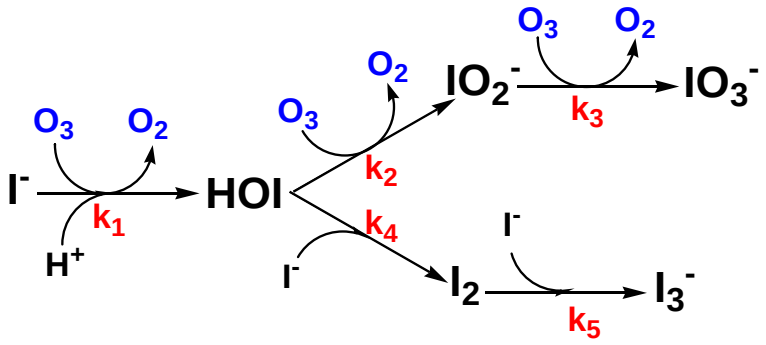

Scheme 3.2. Schematic diagram of the spraying chamber, O_3 (g) injection, and mass spectrometer sampling inlet.